Using water vapour and N2 isotherms to unveil effects of SCMs on nanopores and evaluate hydration degree

(article starts on next page)

Using water vapour and N_2 isotherms to unveil effects of SCMs on nanopores and evaluate hydration degree

Liming Huang [a,b,*], Luping Tang [a,**], Lars Wadsö [c], Ingemar Löfgren [a,d], Nilla Olsson [e], Zhenghong Yang [b,***]

[a] Department of Architecture and Civil Engineering, Chalmers University of Technology, 41296 Gothenburg, Sweden
[b] School of Materials Science and Engineering, Key Laboratory of Advanced Civil Engineering Materials Ministry of Education, Tongji University, Shanghai 201804, PR China
[c] Lund University, Division of Building Materials, 22100 Lund, Sweden
[d] Thomas Concrete Group AB, Södra Vägen 28, 41707 Gothenburg, Sweden
[e] NCC Building, Division Building Sweden, 17080 Solna, Sweden

ABSTRACT

Nanopores are critical for the durability of cement-based materials, but the refinement of these pores by SCMs is yet to have a clear understanding. This paper studied effects of the water–binder ratio, SCMs and the drying on the distribution of nanopores using water vapour and N_2 sorption isotherms. Results show that data of water vapour sorption can be used for a practical evaluation of the hydration degree of SCMs with thermodynamic simulation. Fly ash increases the volume of large gel and capillary pores. It lowers the difference between the sorption of water vapour and N_2. Slag evidently refines the nanopores by increasing the volume of ink-bottle gel pores with an interlayer-size neck. A higher w/b produces more large pores to reduce the effect of drying. Removal of water induces contraction of interlayer and reduces gel pores volume, which causes large difference between sorption of water vapour and N_2.

1. Introduction

Hardened cement-based materials have a porous structure with a wide range of pore sizes from about 5 Å [1] up to the millimeter level (induced by the entrained/entrapped air). Pores of different sizes play different roles in determining the performance of concrete, including the mechanical properties, dimensional stability and durability [2]. The mesoscale pores, mainly existing in calcium silicate hydrate (C-S-H), control the durability such as shrinkage and creep [3], as well as moisture transport in the unsaturated matrix [4]. The complexity of the mesoscale structure of C-S-H is the main obstacle to get a fundamental breakthrough in a general description of the composition–structure–property relationships from the molecular building block view [5]. Therefore, a credible characterization of the nanopores is significant for the assessment of concrete performance, and for a further understanding of the correlation between structure and properties.

To reach the goal of reducing emissions in the cement industry, increasing amounts and diversity of supplementary cementitious materials (SCMs) are used in modern concretes. It is well known that SCMs influence the properties, e.g. the mass transport in cement-based materials [6,7]. However, there are still many gaps in correlating the microstructure of hardened cement-based material with its transport properties, especially for mixtures with the addition of SCMs. It has been found in our previous investigation [4] that slag and fly ash induce a large reduction in the chloride migration and moisture transport in unsaturated paste, without having much effect on the total porosity. The main differences seem to occur in the connectivity of nanosized pores. A clear picture of nanopores in non-dried blended pastes will facilitate the understanding of how SCMs impact the durability properties which are related to the refined pore structure.

Many methods have been applied in the characterization of the nanoscale structure of cement-based materials, covering adsorption

* Corresponding author at: Department of Architecture and Civil Engineering, Chalmers University of Technology, 41296 Gothenburg, Sweden.
** Co-corresponding author at: Department of Architecture and Civil Engineering, Chalmers University of Technology, 41296 Gothenburg, Sweden.
*** Co-corresponding author at: School of Materials Science and Engineering, Key Laboratory of Advanced Civil Engineering Materials Ministry of Education, Tongji University, Shanghai 201804, PR China.
E-mail addresses: limingh@chalmers.se (L. Huang), tang.luping@chalmers.se (L. Tang), tjzhy92037@163.com (Z. Yang).

isotherms of N_2 [8] and water vapour [9–11], small-angle X-ray scattering [12,13], small-angle neutron scattering [14], low-field proton NMR [15–17], and mercury intrusion porosimetry [18]. A treatment to remove the water in the materials is required in most of these measurements. Currently, there is no such method that can remove the non-bound water without damage to the structure of the C-S-H. During the process of water removal (drying process), the mesoscale pore structure [19,20] and the chemical structure after a certain extreme drying [15] will be altered due to the change of forces and interactions in the matrix. For measuring the mesoscale pores, the most widely-used methods are the sorption isotherms of N_2 and water vapour (static or dynamic [11,21]). Several publications reported effects of different drying methods on the pore structure by N_2 adsorption [8,22]. Water vapour sorption has been considered as the most suitable approach to reveal the microstructure of the cement-based materials in a full scale [9]. The specific surface area (SSA) measured by water vapour sorption is generally larger than that by N_2 sorption by a factor, in some drying conditions, of up to 10 times or more [23–27]. Odler [26] explained that the lower SSA by N_2, compared to water vapour, is mainly due to the extremely limited accessibility of nitrogen molecules into the small pores, but there was no clear indication about the critical pore size that is accessible for N_2. Jennings and Thomas [28] discussed the publication by Odler [26] to stress that a part of the pores in low density (LD) C-S-H is hard for N_2 to access as well. However, they had a consensus that the ratio of high density (HD) C-S-H and LD C-S-H would influence the difference in SSA by these two methods. The incorporation of SCMs will modify the structure of the main hydration products, including the ratio of these two C-S-H [29]. One part of this paper aims to have a comprehensive assessment of effects of SCMs on the differences in the measured pore structure by water vapour and N_2 sorption.

The amount of HD and LD C-S-H, which most possibly relates to the inner and outer products [30,31], depends on the hydration degree of the cement and SCMs. Hydration degree is an important index of cement-based materials, which correlates to not only the mechanical performance but also the durability of concretes. For Portland cement, the degree of hydration can be assessed by the consumption of crystal mineral in clinker, which can be calculated by Rietveld analysis of X-ray diffraction data [32]. However, it is much more complicated when the binders contain amorphous SCMs phases. Scrivener et al. [33] summarised most of the methods applied for measuring the hydration degree of SCMs, and all the methods with a good rating require either access to advanced equipment (such as NMR) or a highly professional skill in the data analysis (PONKCS method). This paper will propose an easy-to-perform method to determine the hydration degree of SCMs at later ages by using water vapour sorption data to calculate the C-S-H content [11,34] and simulation by GEMs software (an open access source).

The effect of SCMs on the nanopores of hardened pastes has been investigated in this study. Pore structure information was analysed in detail based on the data from dynamic water vapour sorption (DVS) and nitrogen sorption isotherms (NS). The pore size distribution (PSD) in hardened pastes was calculated by the Barrett–Joyner–Halenda (BJH) model with the data from DVS and NS. The content of C-S-H was determined from the DVS data, and thermogravimetric analysis (TGA) was applied to determine the portlandite content. The hydration degree of SCMs has been evaluated by the C-S-H and portlandite content coupled with GEMs simulation. Finally, a comprehensive discussion is presented to understand the underlying mechanism of the differences in water vapour and N_2 sorption equilibrium process. The advantages and limitations of the proposed method for the hydration degree evaluation are addressed in the discussion part as well.

2. Materials and methods

2.1. Preparation of samples

Cement (CEM I 52.5 R) with a Blaine surface of 525 m^2/kg was used

in this investigation. Two different kinds of SCMs (ground granulated blast furnace slag and fly ash) and limestone were used to replace part of Portland cement to produce the blended pastes. Detailed information on the slag (SL), fly ash (FA) and limestone (LL) powder is described in [35]. Table 1 presents the mass proportions of the 11 samples. The pure CEM I (noted as P0) was used as the reference binder. CEM I was partially replaced by 35 % FA (noted as P1) or SL (noted as P2) to obtain a binary binder system. A ternary system (noted as P3) was made by replacing cement with 35 % SL and 16 % LL. P0, P2 and P3 were mixed with water–binder ratios (w/b) of 0.35, 0.45 and 0.55, respectively. P1 was mixed with a w/b of 0.35 and 0.45. The procedure for mixing is described in detail in [36].

Samples were cast in zip bags (150 mm × 200 mm). In order to easily crush the hardened pastes into small particles, the fresh pastes were rolled into a plate shape with a thickness of about 1 mm before the bags were sealed. All samples were taken out and crushed into small particles with a diameter of about 1 mm after a sealed curing for 1 week. Afterwards, the particles were cured in water for 6 months in a sealed box (1 l), and the mass of the curing water was controlled (about 15 % of particles mass) to provide enough moisture but avoid too much leaching. A part of each sample was then conditioned under 11 % relative humidity (controlled by the saturated LiCl solution) for 1 year. The temperature of the curing and mixing environment was constant at 20 ± 1 °C.

2.2. Dynamic water vapour sorption isotherm

The 6-month wet cured samples were used to measure the vapour desorption isotherms. The dynamic vapour sorption isotherm was performed in a gravimetric water vapour sorption instrument, DVS (Advantage, Surface Measurements Systems, UK). In this, the mass of small samples is continuously recorded during their exposure to different relative humidity (RH) conditions. Samples of 40–60 mg were exposed to an RH-sequence (95 %–90 %–80 %–70 %–50 %–40 %–35 %–30 %–20 %–10 %–0 %) at 20 °C. Each RH step required a duration of 30–60 h to reach the criterion of mass loss rate lower than 0.0001 %/min. For each mix, we measured at least two samples and the results are an average of parallel measurements.

2.3. Nitrogen sorption

A BET instrument (TriStar3000, Micromeritics) was used to measure the nitrogen sorption isotherm of samples that were dried under 11 % RH for 1 year. Before the sorption measurement, samples had been outgassed for 4 h with a continuous N_2 gas flow at 60 °C for a fast water removal [22]. Adsorption isotherms were measured over the pressure range of 0.01–0.982 P/Po with an equilibrium interval of 10 s for each step at 77 K. Each sample has been repeated at least once, and the final value is an average of parallel tests.

Table 1
Mix proportions of 11 different samples by weight percentage.

Samples	Binders				w/b
	Cement	Fly ash	Slag	Limestone	
P035	100 %	–	–	–	0.35
P045					0.45
P055					0.55
P135	65 %	35 %	–	–	0.35
P145					0.45
P235	65 %	–	35 %	–	0.35
P245					0.45
P255					0.55
P335	49 %	–	35 %	16 %	0.35
P345					0.45
P355					0.55

2.4. Thermogravimetric analysis

The weight loss due to the decomposition of portlandite was measured by a thermogravimetric and differential thermal analysis instrument (SDT Q600, TA Instruments) with a Stanton Redcroft STA 780 simultaneous thermal analyser. Powder samples (dried at 11 % RH for 1 year) were heated at a rate of 10 °C/min under a continuous nitrogen flow (100 cm^3/min) from 20 °C to 1000 °C.

2.5. Thermodynamic simulation

Thermodynamic modelling was performed using an open access software-free Gibbs Energy Minimization program GEM-Selektor v3.7. The simulation was based on the cement database Cemdata18 [37] combined with the PSI-GEMS thermodynamic database [38]. The effects of different SCMs on the phase assemblage of products were analysed by assuming that clinker has a hydration degree with 92.2 % after a 6-month water curing at 20 °C (based on portlandite content by TGA). This value is very close to the value reported in [39] with similar clinker composition and curing condition.
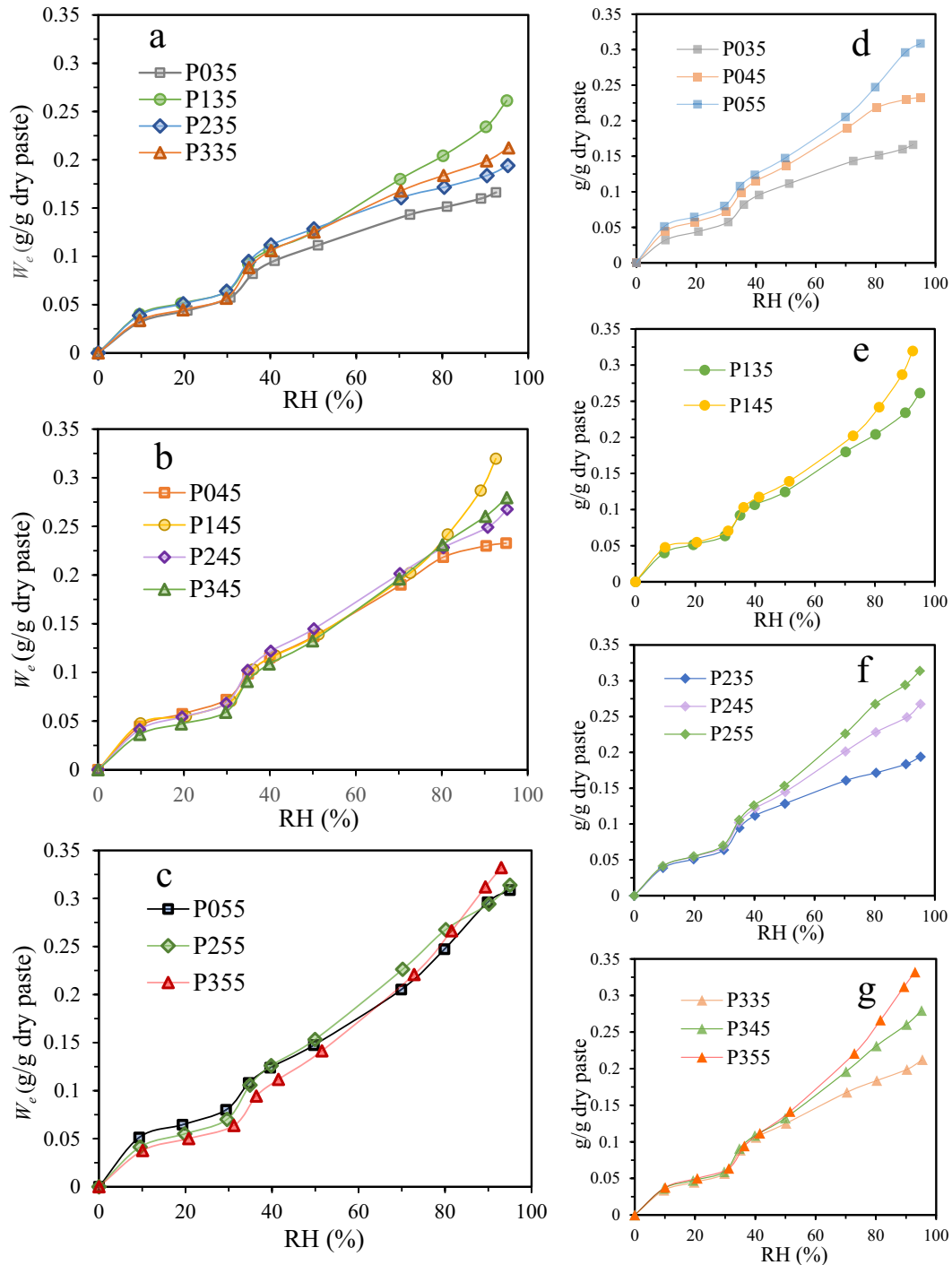

Fig. 1. Water vapour desorption isotherms of all the 11 samples measured at 20 °C. Plots in a, b and c are comparisons between different binder systems with the same w/b. Plots in d, e, f, and g are comparison between different w/b ratios with the same binder system.

3. Results

3.1. Water vapour desorption isotherms

Water vapour desorption and adsorption isotherms were used for modelling moisture transport, understanding the mechanism of drying shrinkage [40,41], and microstructural changes during the drying process [9]. Fig. 1 shows the water vapour desorption isotherms of hardened cement-based pastes (hcps). With the same *w/b* of 0.35, the replacement with SCMs increases the moisture content (W_e) in the hcps under all RH conditions. Due to the refinement effect of SCMs, both the vapour diffusion and total moisture transport coefficient of the blended pastes will be much lower than that of CEM I paste [36]. These dual effects induce a longer drying time for the modern concretes (blended with SCMs) than for the ordinary cement concretes, something which deserves special attention for the application of SCMs in buildings.

When pastes were mixed with the *w/b* of 0.45, the blending of 35 % FA seemed to have a minor effect on the moisture content below 70 % RH. This is consistent with the findings in [42], where the paste was cured under a sealed condition for 6 months. At RHs above 70 %, the blended pastes contain more moisture than the CEM I paste, and the differences between the blended pastes and CEM I pastes increase as the RH gets higher.

An increase in *w/b* to 0.55 reduces the difference between the moisture content in the SL blended pastes (P2 and P3) and that in the CEM I paste (P0) (see Fig. 1c) at RH above 70 %. The ternary paste (P355) has the lowest moisture content in RH below 35 %. Fig. 1d shows that an increase in *w/b* induces moisture content in CEM I pastes at all RH conditions. However, the increase in moisture content of the blended pastes mainly occurs at RH above 40 % as the *w/b* increases. Olsson et al. [43] reported a similar phenomenon in well-hydrated (water curing for 4 years) slag blended pastes.

Moisture capacity (φ) has been defined as the derivative of the moisture content with respect to RH [44]. It is an important parameter to describe and model the moisture transport in cement-based materials. The average moisture capacity ($\overline{\varphi}$) in certain RH intervals is calculated by Eq. (1). W_{ei} and W_{ej} correspond to the moisture content in hcps at RH_i and RH_j, respectively.

$$\overline{\varphi} = \frac{W_{ei} - W_{ej}}{RH_i - RH_j} \tag{1}$$

Fig. 2 presents the comparison of the average moisture capacity of different hcps. For pastes with *w/b* of 0.35 and 0.45, the difference in moisture capacity occurs in the RH intervals of 30 %–36 % and at RHs above 50 %. In general, the blending of SCMs will increase the moisture capacity in these ranges, and FA presents the largest increase. The sudden drop of moisture content from RH of 36 % to 30 % has been explained as the occurrence of cavitation during the drying process [45,46]. The cavitation-induced moisture capacity is higher in the blended pastes than in the CEM I pastes at all *w/b* mixtures. This is due to the refinement of the pore structure, which will be discussed in a later section. A further replacement of cement by LL increases the moisture capacity of pastes with all *w/b* at RHs above 60 %, compared with the binary SL blended pastes.

3.2. The specific surface area by BET method

SSA of the wet and dried pastes was calculated from the water vapour desorption and N₂ adsorption data, respectively, based on the BET theory [47]. The adsorption data up to P/P_0 of 32 % were used for the regression based on Eq. (A) in [47], which works well to describe a unimolecular adsorbed layer. A detailed illustration of the calculation process can be found in a publication by Belie et al. [11].

Table 2 shows the SSA from water vapour desorption (S_w), N₂ adsorption (S_N) and the ratio between them (S_w/S_N). It is evident that an increase of *w/b* from 0.35 to 0.55 causes an increment in both S_w and S_N
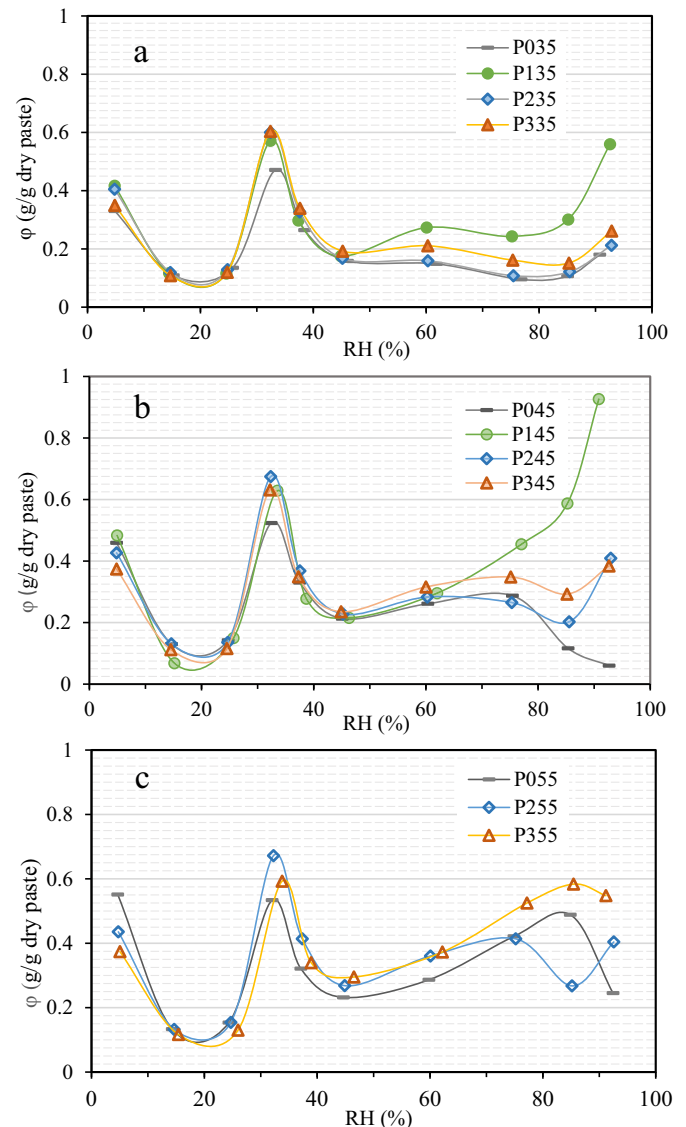

Fig. 2. The average moisture capacity at different RH intervals: a –*w/b* of 0.35; b – *w/b* of 0.45; c – *w/b* of 0.55. Note that the x-coordinate is the average value of the two ends of the RH interval.

Table 2
The surface area of hcp based on water vapour desorption and N₂ adsorption by BET method.

Samples	Specific surface area (m²/g)		S_w/S_N
	N₂ adsorption	Water vapour desorption	
P035	15.2 (±0.5)	162.6	10.7 (±0.4)
P045	21.9 (±0.2)	200.3	9.1 (±0.1)
P055	25.6 (±0.3)	221.5	8.7 (±0.1)
P135	18.5 (±0.6)	183.3	9.9 (±0.3)
P145	25.0 (±1.5)	218.4	8.7 (±0.5)
P235	14.6 (±0.6)	160.1	10.9 (±0.4)
P245	17.4 (±1.3)	192.0	11.1 (±0.8)
P255	22.0 (±0.7)	218.9	9.9 (±0.3)
P335	14.1 (±1.7)	160.1	11.5 (±1.4)
P345	19.4 (±1.3)	187.1	9.7 (±0.6)
P355	23.7 (±0.4)	216.9	9.1 (±0.2)

of all binder systems. It should be noted that S_N is rather lower than the typical value of hardened cement-based materials due to long conditioning time and 60 °C drying. The blending of SL shows a slight

reduction in both S_w and S_N, and the difference is very small when the deviation is considered. A further blending of LL weakly increases the S_N, but it slightly decreases the S_w of hcp with *w/b* of 0.45 and 0.55. FA binary pastes have a higher SSA than the CEM I paste with the same *w/b*. The S_w of wet pastes is in the range of 8–13 times higher than S_N of the dried pastes. The blending of FA seems to decrease this difference, but SL increases it of hcp with *w/b* of 0.45 and 0.55.

A large difference in the S_w and S_N of cement-based materials has been found in many of the previous investigations [11,23,25–27,48–50]. A similar phenomenon was also reported in montmorillonite [51], for which the ratio between S_w and S_N reached as much as 15 due to the swelling of the basal space during wetting (or contraction during drying) of natural montmorillonite [52]. There is no such difference in the S_w and S_N of building materials with other binders such as gypsum, lime or autoclaved lime and silica [24,53]. C-S-H, as the main hydration product of Portland cement-based materials, has a similar structure to that of clay (such as montmorillonite), so it is sensitive to the water content [20]. During the drying treatment of samples for the N_2 sorption test, the interlayer space will be narrowed due to the removal of water [54–56].

Moreover, a long drying process also induces a polymerisation of silicon chains and changes the chemical structure [57,58]. After the nanosized space has contracted to some level or been blocked by chain connections, it is inaccessible for the N_2 molecule. Even though some part of the small layer space is thermodynamically accessible for N_2, its diffusion rate is rather lower than that of water vapour. The large difference (water vapour at 20 °C and N_2 at −196 °C) in the temperature of the measuring environment will affect the equilibrium time, but it may not be the main factor. A further detailed discussion will be given in Section 4.1, which is different from some statements in [11,27].

Fig. 3 shows a typical comparison of the sorption of water vapour in wet hcp and N_2 in long-time dried hcp, exemplified with P0 and P1. An increase in *w/b* induces a higher adsorption of N_2, but it induces minor effects on the water vapour desorption of the blended pastes (P1, also see P2 and P3 in Fig. 1). Within the pressure interval (P/P_0 below 32 %), where the data are used for SSA calculation, the adsorption of water molecules in hcp is >10 times higher than that of N_2 molecules in the dried hcp. However, the surface area occupied by a single N_2 molecule is only about 1.4 times as large as that by a single water molecule (0.162 nm^2 for N_2 and 0.114 nm^2 for H_2O [27]). Therefore, the difference between S_w and S_N is caused by a much lower adsorption of N_2 in the dried pastes than that of water vapour in wet pastes. When C-S-H was dried at RH of 11 %, about 0.7 mol H_2O would be added to the C-S-H structure at the D-dry condition (1.7CaO·SiO$_2$·[1.3–1.5]H$_2$O) [59,60], so we can deduce that the adsorbed water in C-S-H under 11 % RH is about 3.84×10^{-3} mol/g dried mass. The magnitude of this value is in a good match with the adsorption of water vapour in Fig. 3a. The water sorption in

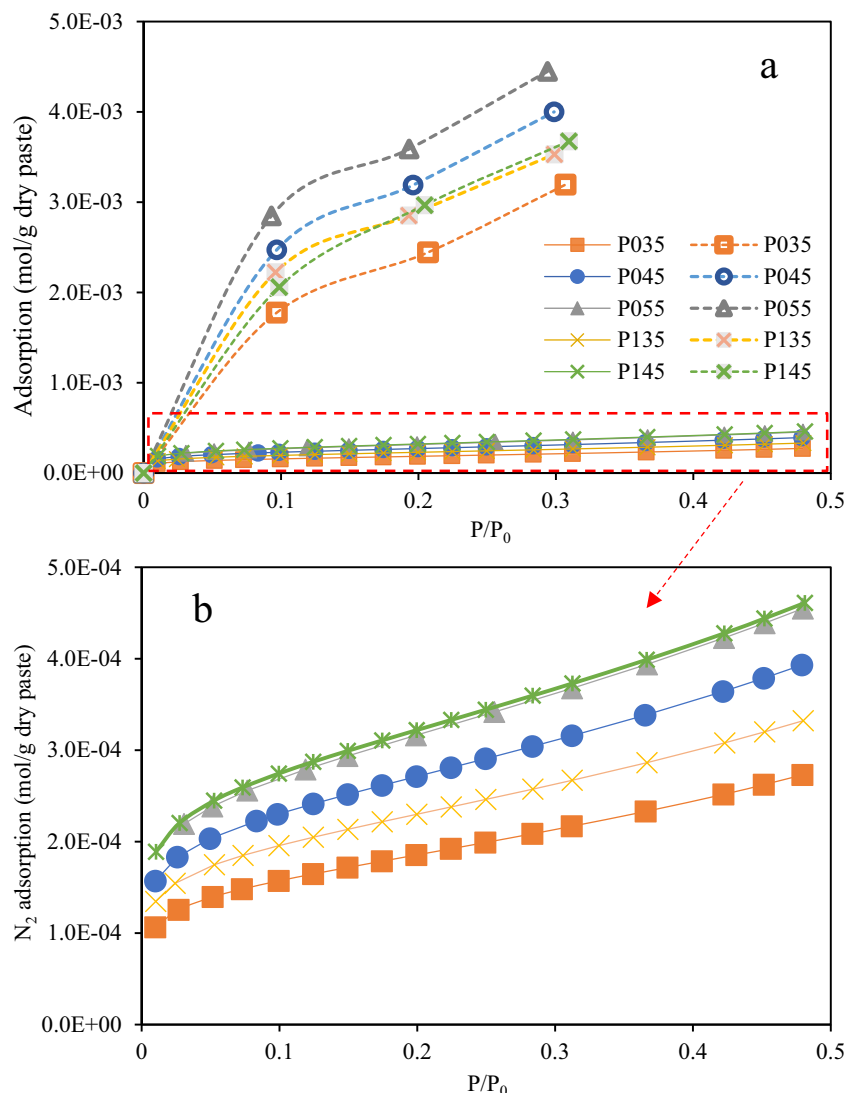**Fig. 3.** Typical comparison of the sorption of water vapour and N_2 in hcps: dashed line – water vapour desorption; solid line – N_2 adsorption.

hcps is lower because some other hydration products also contribute to the weight of dried hcps other than C-S-H. Provided that N_2 could penetrate the layer space of the C-S-H, the adsorbed amount should be of the same order as the water vapour. However, the amount of adsorption indicates that almost no N_2 penetrates the interlayer space of C-S-H.

3.3. Pore size distribution by the BJH method

3.3.1. Effect of ions in pore solution on PSD by DVS

The BJH method was first proposed by Barrett, Joyner and Halenda [61] to calculate the pore size distribution in porous substances based on N_2 isotherms. This model was also widely applied for the determination of PSD in cement-based materials using water vapour desorption data [10,11,41]. Although the pore shape in hcps is more complex than the assumed cylinder shape in this method, and cavitation occurs during the desorption process [45,46] (corresponding to one peak in Fig. 4), the calculated results provide meaningful information for a comparative investigation such as this study.

The Kelvin equation Eq. (2) has been used in the BJH method to describe the correlation between the relative humidity (equilibrium gas pressure P/P_0) and the radius of the condensed liquid in the cylinder pores (r_k).

$$ln RH_k = -\frac{2\gamma V}{r_k RT} cos\theta \qquad (2)$$

where RH_k is the relative humidity value that results from the curvature effects of the menisci at liquid/vapour interfaces. γ is the liquid surface tension (7.28×10^{-2} N/m at 20 °C), V is the molar volume of liquid (1.798×10^{-2} l/mol for water), R is the gas constant (8.314 J/K/mol), T is the absolute temperature of the sample and θ is the contact angle between the liquid and pore wall (assumed to be 0).

However, the equilibrium pressure at the plane surface (p_s) of the solution will be influenced by the ions in the solution. The correlation between the ion concentration and relative humidity at the plane surface (RH_s) is empirically expressed by Raoult's law [62,63], as shown in Eq. (3). n_w is the moles of water in the solution and n_i is the total moles of ions in the solution. Therefore, the observed relative humidity value (RH_o) is a combination of curvature and ion effects, which can be described as Eq. (4).

$$RH_s = \frac{p_s}{p_0} = \frac{n_w}{n_w + n_i} \qquad (3)$$

$$RH_o = RH_k RH_s \qquad (4)$$

The ion concentration in the pore solution was calculated with the chemical composition and water content, which has been previously illustrated in [35]. Herein, we subtracted the alkali ions in the C-S-H by taking the adsorption coefficient of 1.2 % for Na and 2 % for K [64], respectively. The C-S-H content was determined based on the water content at 20 % RH, which will be described in Section 3.4.1. Water content decreases with the lowering of RH, and Raoult's law is only valid for dilute solutions. Therefore, to simplify the analysis we use the water content in naturally saturated pastes (under the sealed curing) to calculate the ion concentrations.

The previous studies [10,11,41] ignored the effect of ions on the RH_s of the pore solution, and they used the observed RH_o as RH_k. Fig. 4 shows the comparison of the calculated PSD with the RH_s of the pore solution and pure water. The ions in the pore solution seem to have a weak effect on the calculated pore width and volume of pores with diameter < 10 nm. However, the omission of ion effects will severely underestimate the size and volume of capillary pores (width > 20 nm). Therefore, it is necessary to include the effect of ions on the RH_s of the pore solution during the calculation of the PSD by using the BJH method on water vapour desorption isotherms.

3.3.2. Comparison of pore size from DVS and NS

On the pore surfaces, there is a physically adsorbed layer of molecules with a statistical thickness t [48,61]. The radius of an open cylinder pore (r_p) is a sum of r_k and t ($r_p = r_k + t$). The correlation between the statistical thickness of the water film and RH in hcp was first reported by Hagymassy et al. [48]. Badmann [65] introduced Eq. (5) to describe the correlation by using two parameters K_1 and K_2. These two parameters are dependent on the composition of the materials. Therefore, we used a trial-error method to adjust the constants for different binder systems. The optimum parameters are obtained by getting a good match between

Table 3
The coefficient of the *t*-curves for different binder systems, representing a *w/b* of 0.35.

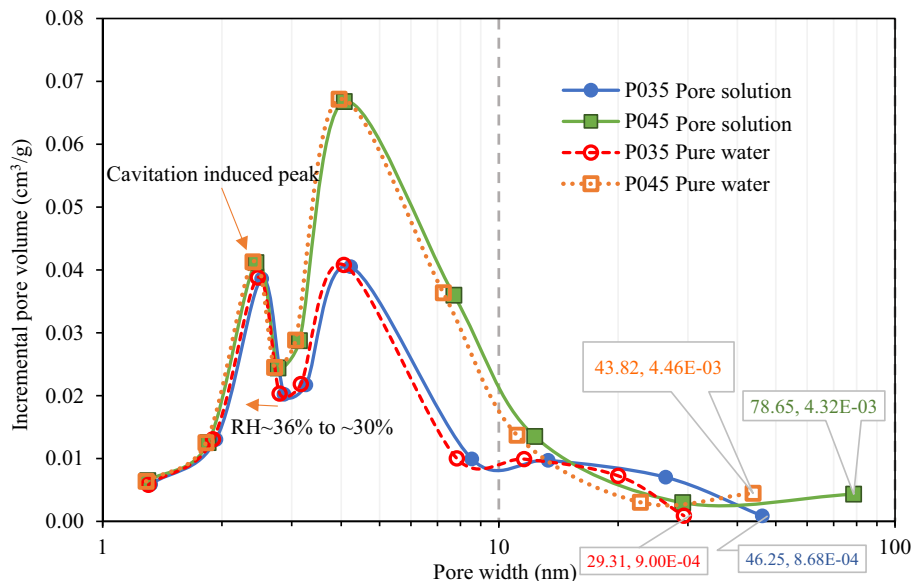| Coefficients	P035	P135	P235	P335
K_1	3.51	2.86	3.20	2.55
K_2	−1.89	−2.10	−2.50	−2.00

Fig. 4. The effect of ions in pore solution on the calculated PSD of hcps.

the measured and calculated total pore volume. Table 3 presents the optimum parameters for 4 different binder systems with all *w/b* (exemplified by a *w/b* of 0.35). Fig. 5 shows the *t*-curves of the different binder systems. It seems that the CEM I paste has the highest thickness of water films at RHs below 50 %, and the SL binary paste increases to be higher than CEM I paste at RH above 50 %. The ternary pastes have the thinnest water film. However, the differences between binder systems is minor, which is consistent with the reported value in [48].

$$t(RH) = K_1 + K_2(ln(-ln(RH)))$$ (5)

Fig. 6 shows the PSD by analysing the water vapour and N_2 sorption data with the BJH method. The calculated pore widths (diameter of open cylinder pores) are in a range of 1–90 nm, so the pore structure at mesoscale can be effectively indicated by the water vapour desorption data. According to the classification by Jennings in [9], the moisture below 25 % RH corresponds to the water in the interlayer space. The calculated pore width (including the t thickness) is approximately 1.66 nm at ~20 % RH. Referring to the definition in Jennings' colloidal model [66], the moisture in spaces of this dimension includes the water in the interlayer space, intraglobular pores (to 1 nm) and small gel pores (1–3 nm). Without consideration of the water film (t thickness), the pore width filled at ~20 % RH is about 1.2 nm. The ^1H NMR results from Muller et al. [67] indicated that there is no distinguishing signal between the water in the interlayer space and intraglobular pores, so they classified the pore space up to 1 nm as interlayer space. Therefore, we classified the moisture up to 20 % RH as water in the interlayer space in this study (see Fig. 6a).

Moisture desorption between 20 % and 40 % RH induces a peak in the incremental volume of pores with sizes between 1.66 and 3.3 nm. The moisture change in the range of 25 %–50 % has been designated as water in SGP or in HD C-S-H [9]. However, a sudden drop between 36 % and 30 % RH is due to the cavitation in larger pores during the drying process. The capillary tension in ink-bottle pores with small necks increases to a very large value, with which pressure cavitation (homogeneous nucleation of bubbles of vapour) could occur. This phenomenon is commonly observed in the N_2 [68] and water vapour desorption [45,46] curve of materials with the complex mesoscale pores. Maruyama et al. [45] found no cavitation in pores smaller than 5 nm (6.4 nm including the *t* thickness) during the desorption of cement-based materials at 20 °C. Thommes et al. [69] reported that the cavitation occurs in pores wider than 8.5 nm during N_2 desorption of mesoporous silicas, and it shows no dependence on the pore shape, pore size or the neck size (at least for necks smaller than 2.6 nm). Rastogi et al. [46] stated that cavitation occurred in the gel pores (in a range of 2–8 nm) of the inner product. Based on these findings, we suggest that the moisture loss from

40 % to 20 % RH is the water in SGP and the ink-bottle LGP connected with the interlayer space. It is meaningless to designate the volume at this interval to pores with a specific size, but it is significant for understanding the refinement effect of SCMs by comparing the volume of ink-bottle gel pores from different binder systems.

The moisture loss from 80 % to 40 % corresponds to the water in pores with a diameter of 12.3–3.3 nm, so it can be classified as the volume of the open LGP pores. Moisture in RH of 97 %–80 % is water in capillary pores with a diameter larger than 12.3 nm. This part of the water is closely related to the *w/b* [41], so it can be used to estimate the original *w/b* of the hcp [9].

Fig. 6a–c indicate that the blending of SCMs slightly reduces the volume of interlayer space in hcp within all the *w/b*. Both SL and FA increase the value of the cavitation-induced peaks, which implies a refining of the LGP to reduce the connectivity. The difference between binary and CEM I hcp becomes larger at higher *w/b*. This reveals a more evident refinement effect from SL and FA, resulting in a larger reducing effect on the moisture and chloride transport [7,35,36,43]. The volume of open LGP pores (3.3–12.3 nm) is increased by the blending of SL and FA, and this effect is significant on hcp with a *w/b* of 0.35. The dilution effect of SCMs will induce a higher effective water-to-cement ratio in the blended hcp than in the CEM I hcp, so it will increase the hydration degree of clinker in the binder systems [70,71]. Moreover, the further hydration of FA and SL generates more content of C-S-H, so the volume of LGP is higher in the binary hcp than in CEM I hcp. A further replacement of CEM I by LL reduces the C-S-H content and thus decreases the LGP compared to SL binary hcp. The dilution effect also induces an increase in the volume of capillary pores (12.3–80 nm), and FA has the largest increasing effect on capillary pores in hcp with *w/b* of 0.35 and 0.45.

Fig. 6d–g presents the comparison between the PSD by water vapour and by N_2 sorption of hcp. It shows that the N_2 sorption measurement of hcp dried at 60 °C with N_2 can only detect the LGP and capillary pores. The detected volume of LGP by N_2 sorption is much lower than that by water vapour sorption. The vacuum or high-temperature drying method induces severe damage of the layer structure of C-S-H, so it results in the contraction of the interlayer space and coarsening of some of the gel pores [16,20,72]. In CEM I and ternary hcps, we can observe an evident increase in capillary pores resulting from the coarsening of the gel during the drying treatment in this study.

A mild drying method such as D-drying [8] or a careful solvent exchange treatment [19,22] can minimise the effect of drying on the structure of the hcp to obtain a higher SSA from the N_2 sorption test. Zhang and Scherer [22] reported that the isopropanol replacement method was the best way to preserve the microstructure, and a high SSA (~ 88 m^2/g for OPC pastes with *w/b* of 0.5) could be measured by N_2 sorption of hcp by this drying method. However, the volume of pores with diameter below 4 nm is far smaller than 0.02 ml/g and this value shows no difference at different curing ages (see Fig. 5 in [22]). Although the hcp was treated with the optimum drying method, the interlayer space and a large part of the gel pores have not been measured by the N_2 sorption. The significant difference in PSD by water vapour sorption and by N_2 sorption (see Fig. 6d) is due to not only the effect of drying but also the difference in accessibility of water and N_2 molecules into the small nanosized channels. This will be discussed further in the final section. The volumes of capillary pores in all binder systems, from both water vapour and N_2 sorption measurement, increase as the *w/b* increases from 0.35 to 0.55. However, the increase of *w/b* from 0.35 to 0.45 in CEM I pastes induces a minor increase in the capillary pores, and it mainly increases the volume of LGP.

3.4. Determination of hydration products and hydration degree of SCMs

3.4.1. Determination of the amount of hydration products

As stated in the previous section, the moisture under 20–25 % RH mainly corresponds to the water in the interlayer space of C-S-H.
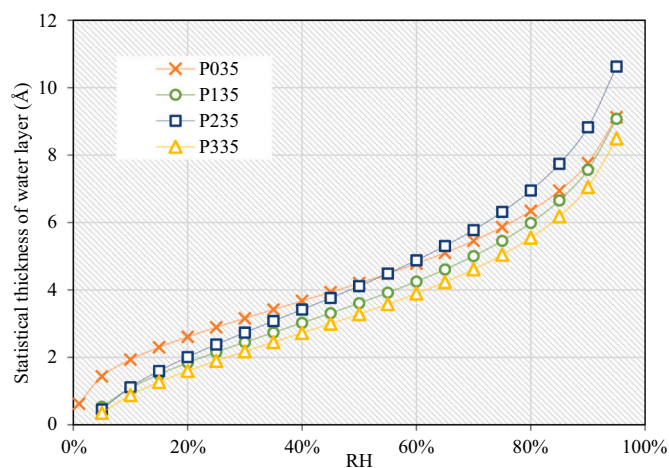

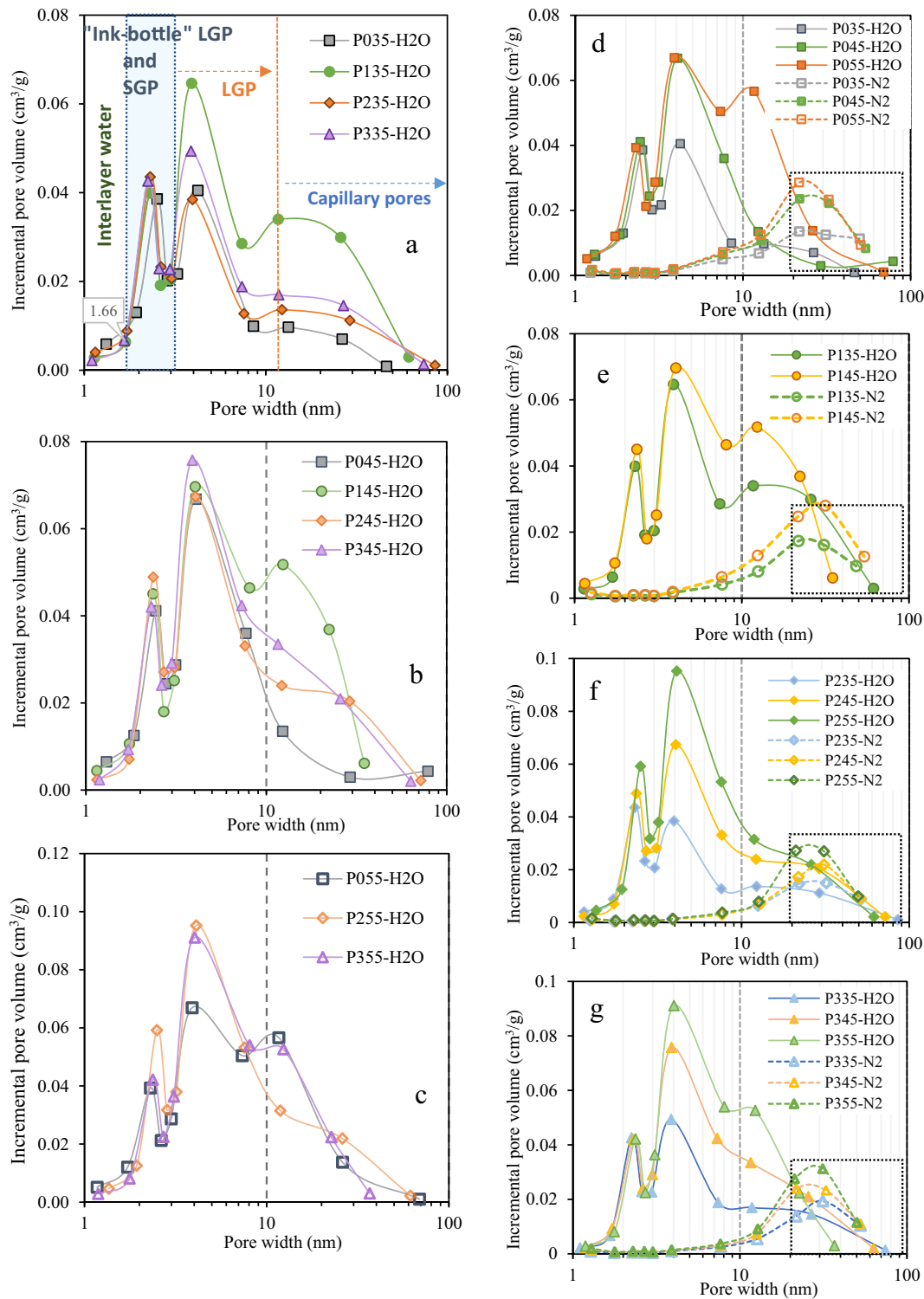**Fig. 5.** Statistical *t*-curves of the adsorbed water film for different binder systems.

Fig. 6. The PSD in hcp calculated by BJH method from water vapour desorption (P***-H₂O) and N₂ sorption isotherm (P***-N2). Graphs a, b and c are the comparison in different binder systems with *w/b* of 0.35, 0.45 and 0.55, respectively. Graphs d, e, f, and g are the comparison in pastes with the same binder system but different *w/b*.

Bonnaud et al. [73] performed a molecule dynamic simulation to reveal the thermodynamics of water confined in the interlayer space, and they found that the interlayer water started to dry at about 20 % RH. This part of the evaporable water is assigned as structural water because its drying will induce irreversible deformation [9]. Due to the unique mesoporous structure of C-S-H, its SSA is at least an order of magnitude greater than any other hydration products [34]. The vast majority of the moisture in hcp is adsorbed in the interlayer space of C-S-H when RH is below the condensation point in the gel pores. Based on the commonly used atomic structure of 1.65CaO·SiO₂·1.75H₂O from [74] or 1.69CaO·SiO₂·1.80H₂O from [75], the evaporable water (dried at ~0 % RH) in the C-S-H structure is approximately 7.3×10^{-3} mol/g (or 0.131 g/g) dried C-S-H with about 0.55 mol chemically bound water attached to Ca or Si atoms [76]. This value is close to the experimentally

measured value (0.1 g/g) in [34] and very close to the value used in [11,41] for calculation of the C-S-H content. if we assume that SCMs have minor effect on the evaporable water in interlayer of C-S-H, Eq. (6) can be used to estimate the C-S-H content in all hcps in this study.

$$W_{CSH} = \frac{n_{e,20}}{\overline{n}_{w,CSH}} \quad (6)$$

where $n_{e,20}$ (mol/g) is the amount of water adsorbed in hcp at 20 % RH (partially shown in Fig. 3 and calculated from Fig. 1), $\overline{n}_{w,CSH}$ is the amount of evaporable water in C-S-H with respect to the dried weight (7.3×10^{-3} mol/g), and W_{CSH} is the weight of C-S-H in the dried hcp.

The amount of portlandite was detected by TGA for assessing the feasibility of evaluating the hydration degree of SCMs by water vapour sorption data. The mass loss in the temperature range of 350–500 °C (m_L) was used to calculate the content of portlandite (Wp) in the dried hcp. M_p and M_w are the molar mass of portlandite and water, respectively. m_{dp} is the weight of the hcp dried at 11 % RH.

$$W_p = \frac{m_L}{m_{dp}} \frac{M_p}{M_w} \quad (7)$$

Fig. 7a shows the calculated C-S-H content in the hcps. P035 has the lowest C-S-H content with a value of 0.351 g/g, due to the limited availability of water in large pores for later age hydration. A w/b of 0.45 provides more water for hydration to induce a significant increase in the amount of C-S-H (to about 0.477 g/g). An increase of w/b from 0.45 to 0.55 can enhance the later hydration to produce the highest content of C-S-H in CEM I hcp among all the mixtures, but this effect is much

weaker than the change due to the increase of w/b from 0.35 to 0.45. This is consistent with the volume of LGP in Fig. 6d, and it implies that the addition of water in CEM I pastes with w/b higher than 0.42 (the critical value for reaching full hydration [77]) has minor effects on the hydration degree at later ages. For hcp with w/b of 0.35, the blended hcps have higher amounts of C-S-H due to the dilution effect of SCMs to increase the effective water to cement ratio. With w/b of 0.45 and 0.55, the blended hcps have lower amounts of C-S-H than the CEM I hcp. The increase in w/b of the blended hcps has a much weaker effect in terms of increasing the C-S-H content compared with CEM I hcp.

Fig. 7b shows that CEM I hcp with w/b of 0.55 has the highest portlandite content with 0.22 g/g, which is about 92.2 % of amount in a fully hydrated CEM I calculated by GEMs (23.87 %). The blending of FA and SL will reduce the portlandite content mainly due to the pozzolanic reaction of FA and latent hydraulic hydration of SL [78], so the previous publication reported that portlandite content in the blended hcp can be used to calculate the hydration degree of SCMs [33]. The increase in w/b facilitates the consumption of portlandite.

3.4.2. The evolution of hydration products by GEMs simulation

Thermodynamic simulations have been widely applied to reveal the effect of SCMs on the hydration and phase assemblage in the hcps. De Weerdt et al. [79] performed such a simulation to understand the effect of limestone on the phase assemblage and volume change of hcp. Schöler et al. [80] applied this method in a quaternary binder system with slag, fly ash and limestone. Lothenbach and Zajac [81] conducted a review on the application of thermodynamic modelling on the blended hcp, and
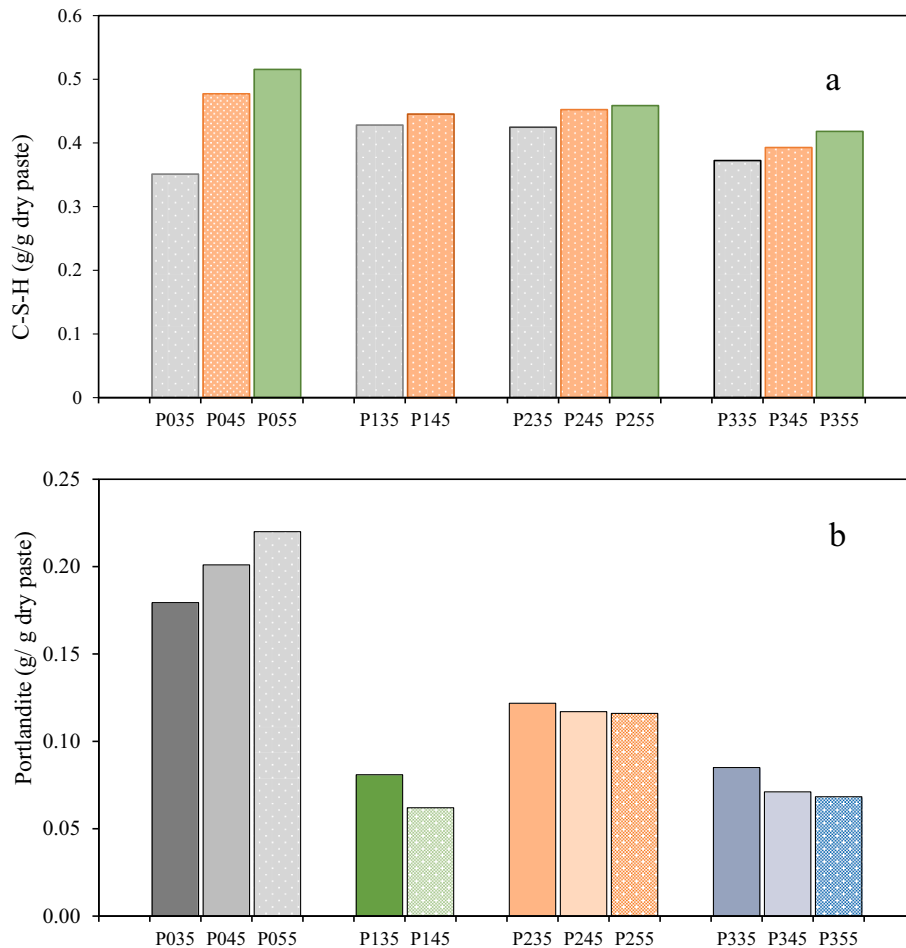

Fig. 7. Amounts of the two main hydration products in hcp: a – the content of C-S-H in hcp calculated by water vapour desorption data; b – the content of portlandite in hcp determined by thermogravimetric analysis.

emphasised that the corresponding models and approaches had achieved a mature level. The increasing availability of thermodynamic data is continuously improving the reliability of thermodynamic calculations on cement-based systems.

Fig. 8 shows the evolution of hydration phases in the hcp with the increase in hydration degree of SCMs (SL and FA). It should be noted that the hydration degree of CEM I has been assumed to be 92.2 %, which is calculated by dividing the measured content of portlandite in P055 (22.0 % by TGA) with portlandite content in the full-hydrated paste (23.87 % by GEMs). For the blended hcp, the lowest effective water-to-cement ratio is 0.53, so it would be reasonable to make such an assumption for clinker in the blended pastes.

The key point for performing a good thermodynamic simulation is to use an accurate database, and to identify the right phases in the hydration products. The presence of Fe and Al in the binder system will form the Fe-siliceous hydrogarnet (Si-hydrogarnet) [82]. The limited amount of limestone in cement (see the composition of CEM I in [35]) will induce the formation of hemicarboaluminate (Hc) and monocarboaluminate (Mc) [79,83]. The blending of limestone will stabilise the Mc, so there is no Hc in the ternary SL system at a later age [84] (also see Fig. 8c). The amount of ettringite, monosulfate (AFm), Hc and Mc is a complex equilibrium related to the amount of calcium aluminate, sulfate, and calcite in the binder system. When the hydration products have an Al/Si ratio higher than 0.1, strätlingite will be present in addition to C-A-S-H [85]. However, strätlingite would form only after all the portlandite has been consumed by the pozzolanic reaction of fly ash [83], and this is not likely to occur in the actual hydration situation.

After taking all these phase formation mechanisms into consideration, the simulation results are reliable for the evaluation of the phases content. The attention is focused on the amount of the two main hydration products, C-S-H and portlandite. For the FA binary hcp, portlandite will decrease due to the consumption by the pozzolanic reaction of FA. In the meantime, the amount of C-S-H will increase with the hydration degree before a complete consumption of FA. Theoretically, a hydration degree of 38 % (13.26 % of FA in the binder system) will consume all portlandite in P145. Above this hydration degree, the content of C-S-H will decrease due to the formation of strätlingite. In the SL blended hcp, the amount of C-S-H shows a gradual increase, while that of portlandite shows an opposite trend, as the hydration degree of SL increases to 1.

3.4.3. Hydration degree of SCMs

With the results in Fig. 8, the amount of C-S-H and portlandite in the dried hcp can be calculated by using Eq. (8). W_{phase} (g/g) is the mass fraction of hydration products, m_{phase} (g) is the weight of hydration products, m_{wp} (g) is the total weight of hcp, and m_{ps} (g) is the weight of the pore solution.

$$W_{phase} = \frac{m_{phase}}{m_{wp} - m_{ps}} \tag{8}$$

Fig. 9 shows the relationship between the hydration degree of SCMs and the amounts of the main hydration products per gram of dried hcp. According to this linear correlation, we can calculate the hydration degree of SCMs by the measured amount of C-S-H or portlandite (see Fig. 7). For the FA binary system, portlandite has not been completely consumed by pozzolanic reaction of FA (see Fig. 7) due to its limited hydration degree. Therefore, the data below a hydration degree of 35 % are used to perform the regression of FA binary hcp.

Fig. 10 shows the hydration degree of FA and SL based on the calculated C-S-H content from DVS and the measured portlandite content from TGA, respectively. A generally good match can be observed between the hydration degree assessed by the C-S-H and portlandite content. This confirms that the estimation of the C-S-H content by water vapour desorption is reliable for assessing the hydration degree. The calculated hydration degree of FA is in a range of 20 %–30 %, and this range matches the previously reported data [33,78,86] for hcp blended

with 35 % FA with a similar curing condition. The determined hydration degree of SL is about 40 %–52 % for binary hcp and 43 %–59 % for ternary hcp. These values are very close to the measured hydration degree of SL blended hcp with the w/b of 0.42 reported in [87], and some minor differences are probably mainly due to the differences in the composition and fineness of the cement or SL. As the w/b increases, the increase in hydration of FA and SL at later ages can be effectively identified by this determination method. Although the increase of w/b from 0.45 to 0.55 has minor effects on the hydration of CEM I, its effect on increasing the hydration of SCMs is evident. This means that the hydration of SCMs at a later age is more sensitive to the availability of moisture in pores compared to cement clinker.

4. Discussion

4.1. Origin of the differences in microstructure measured by water vapour and N₂ sorption

There is a large difference in pore structure of hcp detected by water vapour and N₂ sorption (see Table 2 and Fig. 6). This phenomenon has also been reported in many previous investigations [11,23,25–27,48–50]. However, the underlying mechanism for such a big difference is still not clearly identified. The temperature for the water vapour sorption experiments (normally 20–25 °C) is much higher than that for N₂ sorption (about −196 °C). However, the coefficient of thermal expansion is about 11×10^{-6}/°C for dried concrete [88], so the maximum thermal strain is 0.15–0.2 % after cooling down to −196 °C [89]. This value is considerably lower than the magnitude of difference in the SSA and volume of mesopores by these two methods. Therefore, we can deduce that the effect from thermal strain is negligible.

The microstructure of C-S-H is very sensitive to the moisture content [20]. The drying of the surface water in the electrical double layer will reduce the repulsive force between globules to drive the globules somewhat closer [20,66]. This induces the contraction of SGP and coarsening of LGP (see Fig. 6 and illustration in Fig. 11). Drying treatment also results in a reduction of the hydration and osmotic repulsion forces with the decrease in water films [90]. Therefore, the layer distance will decrease to increase the repulsion for creating a new balance between the attraction and repulsion. Change of colloidal distance reduces the connectivity of the gel pores and the accessible volume for N₂. Furthermore, drying also induces new chemical bonds between globules or at the end of globules [91]. All these effects contribute to the difference in the PSD from water vapour and N₂ sorption, thereby causing an irreversible change of structure in hcp.

The equilibrium state of the sorption measurement impacts the obtained results. A typical C-S-H structure with Ca/Si of 1.65 in [74,75] has a basal space of about 11.8 Å. The free space in the interlayer is about 5 Å [1] in wet C-S-H, and the diameter of the C-S-H globules is about 3–4 nm [66,92]. Ideally, the diffusion at these dimensions may be dominated by Knudsen diffusion because Knudsen number (=3/0.25) is larger than 10 [93]. The kinetic diameters of N₂ and H₂O are 0.364 nm and 0.265 nm for this diffusion process [94], respectively. The severe drying will induce a collapse of the interlayer space by up to about 25 % (a contraction by 0.25 nm) [54–56]. The free layer distance is reduced to about 0.3 nm which is smaller than the kinetic diameters of N₂. This explains why interlayer space is inaccessible for the N₂, and this also means that N₂ cannot get access to the gel pores with an interlayer space neck (see Fig. 11). However, water can re-enter most of the interlayer [9] and hydrate the counterions to induce swelling of the interlayer space [20,52,95].

A mild drying method may make it possible to get a SSA by N₂ of about 100 m²/g for hcp at later ages [22,96], which is much closer to the SSA by water vapour compared with the large difference shown in Table 2. However, the difference in the PSD measured by water vapour and N₂ sorption still exists. Therefore, apart from finding methods to minimise the effect of drying, the reliability of N₂ sorption measurement
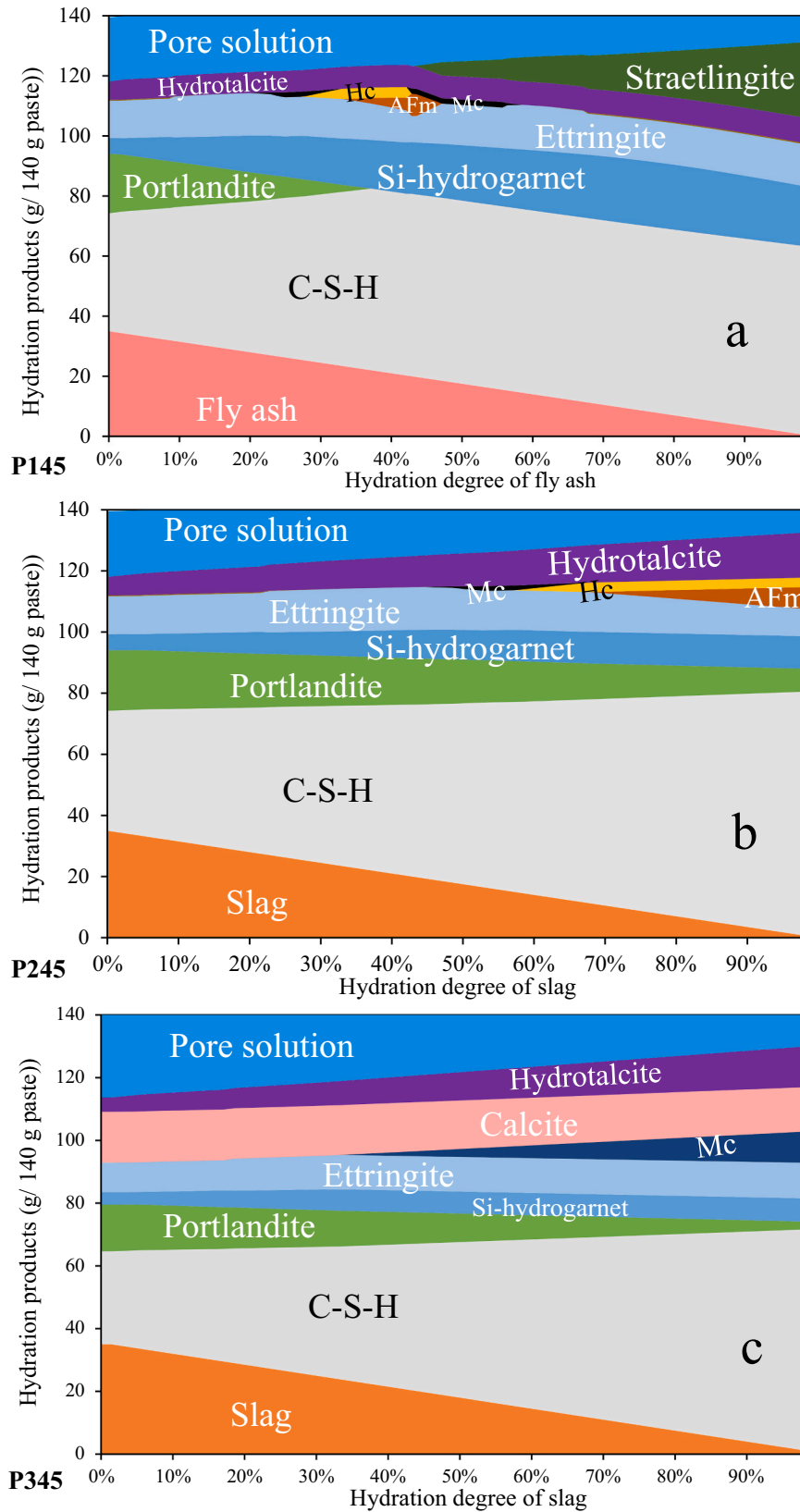
Fig. 8. Phase assemblage of hydration products with the increase in hydration degree of SCMs: a – FA blended binary system; b – SL blended binary system; c – SL and LL ternary system.
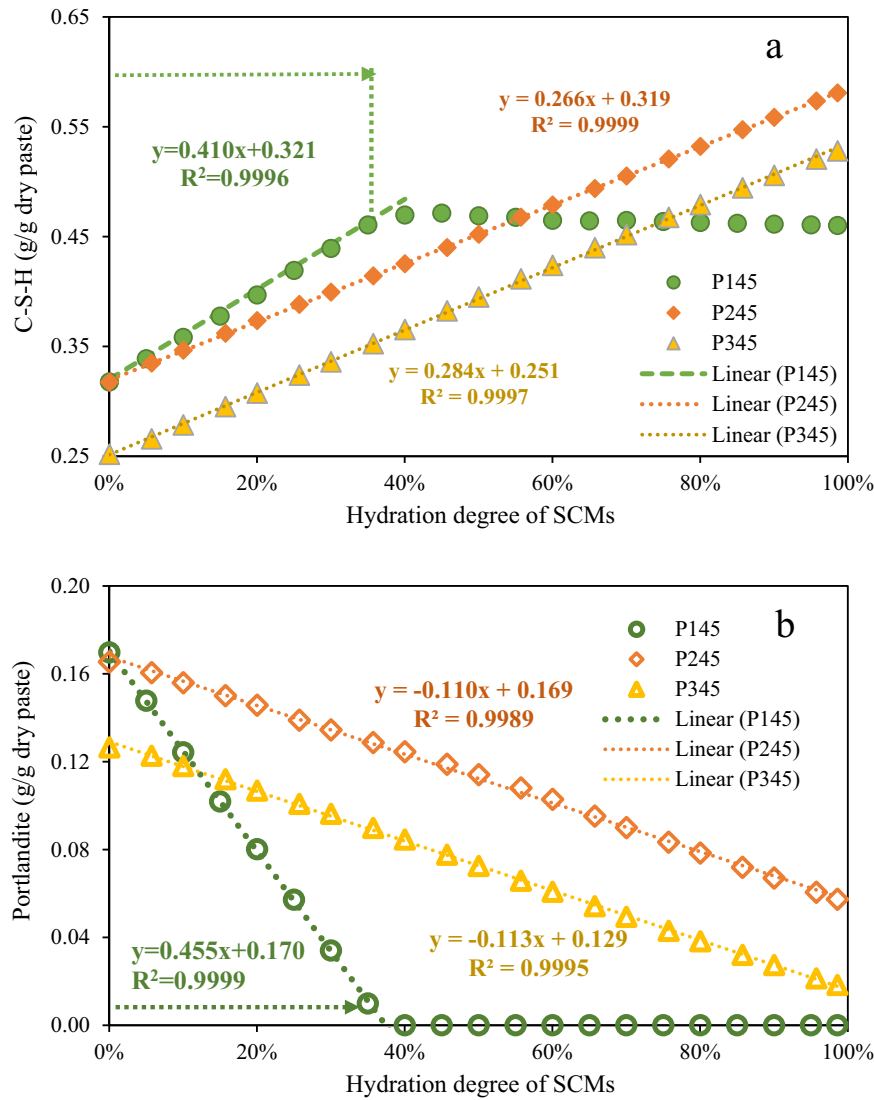
Fig. 9. The relationship between the amount of the main hydration products and hydration degree of SCMs: a – C-S-H; b – portlandite.
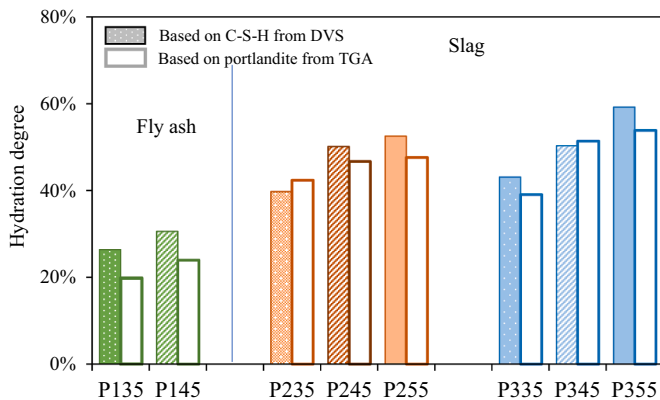

Fig. 10. Hydration degree of FA and SL in the blended hcp after a 6–month water curing.

can be increased by means of improving the equilibrium, such as adjusting the equilibrium time and decreasing the particle size of the sample [97].

4.2. The effect of SCMs

The replacement with SCMs (slag and fly ash) increases the volume of ink-bottle gel pores with small necks (see Fig. 6). Moreover, the hydration products of the SL blended pastes include some Mg-Al layered double hydroxide (LDH) [98] with a layer space filled with water but inaccessible for N_2 after drying. The adsorbed amount of water in LDH is significant because the content of evaporable water is about 40 % with respect to its dry weight [99,100]. These effects will induce a larger difference between the mesoscale pore structure of hcp measured by water vapour and that by N_2 sorption. Therefore, we can observe a higher difference in sorption of water vapour and N_2 in the SL hcp compared with CEM I hcp with *w/b* of 0.45 and 0.55.

The chemical composition of fly ash is rich in Al_2O_3 but lacks CaO. Blending of it will incorporate *Al* into the structure of C-S-H to increase the layer space [85,101]. Meanwhile, it will reduce the Ca/Si ratio markedly, so it results in reduction of counterions in the interlayer space (mainly Ca). The SSA of the well-crystallised 11 Å tobermorite (basal space of ~11 Å, Ca/Si of 1) measured by water vapour [101] is similar to the SSA measured by N_2, with a value of about 76–78 m^2/g [102]. This implies that the contraction of the interlayer space in C-S-H is mainly due to the dehydration of counterions. The decrease in the interlayer Ca will reduce the contraction level of the interlayer space. Furthermore,
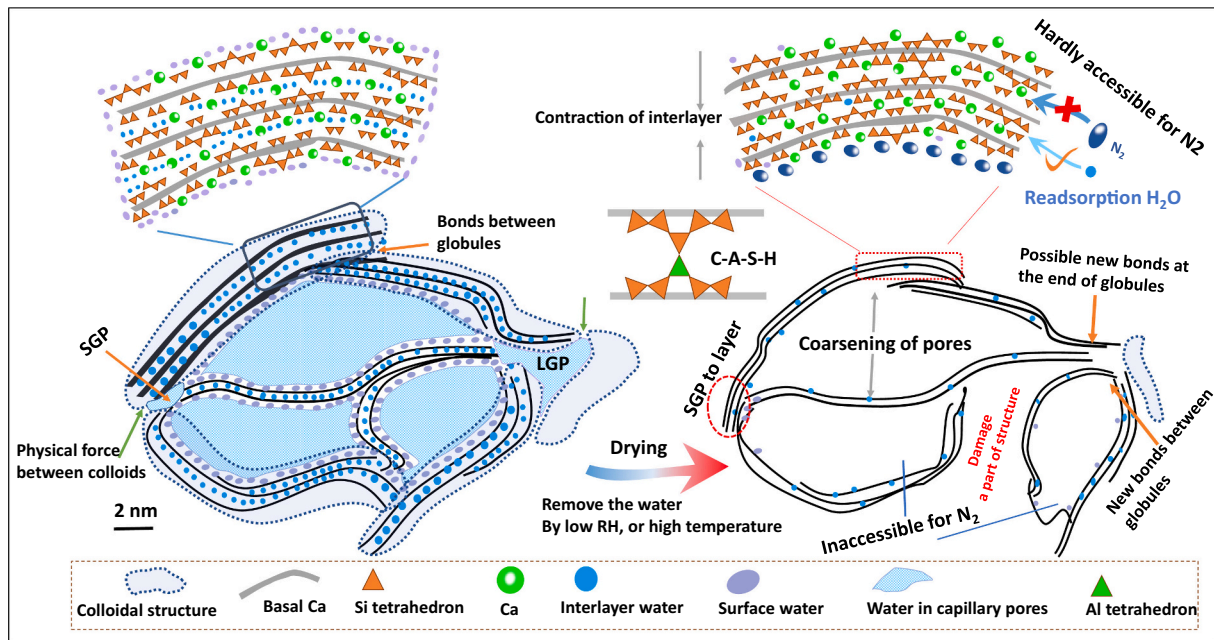
Fig. 11. Illustration of the effect of drying on the C-S-H structure and sorption difference in water vapour and N_2.

incorporation of *Al* will induce some cross-connection between layers by *Al* ions (see Fig. 11), improving the crystallinity of the structure [103], which will also lower the contraction of the layers due to drying.

SCMs increase the volume of LGP and capillary pores (see Fig. 6). This reduces the contribution from the gel pores in the SSA of hcp, so it reduces the effect from SGP and the interlayer after drying. The increase in *w/b* increases the percentage of LGP and capillary pores as well. Therefore, we can observe the decrease in S_w/S_N not only after blending of FA but also with the increase in *w/b*.

4.3. Advantages and limitations in the proposed method

Compared with the previous methods for determining the hydration degree [33], the approach proposed in this paper is easy to perform without the use of advanced equipment if we use the saturated salt solutions for RH control. Furthermore, we can obtain a good indication of the pore size distribution by water vapour sorption. The evaluation of hydration degree of SCMs can be performed as simple as follow:

a. Measuring the weight of samples after an equilibrium at 20 %–25 % RH.
b. Afterwards, drying the samples under ~0 % RH or vacuum dry at room temperature (23–25 °C) to a constant weight.
c. Using the moisture loss from 25 % to 0 % RH to calculate the content of C-S-H with Eq. (6).
d. Performing a thermodynamic modelling to get the hydration products in the system with the increase in consumption of SCMs, and with a certain amount of hydrated clinker.
e. Based on the correlation between hydration degree and C-S-H amount in thermodynamic modelling, we can feed the data in step c to obtain a practical hydration degree of SCMs.

However, if some SCMs have large influences on the hydration of clinker, a method needs to be coupled to evaluate the hydration degree of the cement clinker. This would benefit from further research on developing practical method to measure the unreacted clinker, such as extraction or selective dissolution. This method is strongly dependent on the database for thermodynamic modelling. We did not perform an accurate assessment of the effect of SCMs on the actual Ca/Si of the C-S-H. Slag and fly ash will reduce the Ca/Si in C-(A)-S-H to reduce the water

content in the interlayers. Ignoring this change leads to the underestimation of hydration degree due to the lower calculated C-S-H content based on water vapour sorption. This point will be improved because much research is ongoing to continuously enrich the thermodynamic database [37,81].

5. Conclusions

Dynamic vapour sorption and N_2 sorption isotherms have been used to investigate the effects of the water–binder ratio and SCMs on the mesoscale pore structure of cement-based materials. A novel approach is proposed for an effective evaluation of the hydration degree of SCMs based on water vapour sorption and thermodynamic modelling. Finally, a holistic discussion has been carried out to understand the large difference in the pore structure measured by water vapour and N_2 sorption.

SCMs markedly increase the moisture capacity of hcp at RHs above 50 % due to their effect of increasing the volume of large gel pores and capillary pores. Cavitation will occur during the desorption of water vapour at RH between 36 % and 30 %, which will induce an overestimation of the volume of the small capillary pores. However, the increase in the cavitation-induced value reveals part of the refinement effect of the SCMs. It is essential to include the effect of ions on the equilibrium pressure of water vapour on a plane surface when the BJH model is applied to calculate the pore size distribution. Replacement of CEM I by slag and fly ash increases the volume of both small and large gel pores, and this effect is most evident at the lowest *w/b* (0.35 in this study). The dilution effect from SCMs provides essential extra water for reaching full hydration of the clinker. The estimated content of C-S-H in hcp reveals that the increase in *w/b* clearly promotes the hydration of SCMs at later ages.

Coupled with the thermodynamic simulation by GEMs, the amount of C-S-H calculated from water vapour desorption can be used to perform an effective evaluation of the hydration degree of SCMs. This method can be easily operated without use of expensive equipment, and a reasonable hydration degree of SCMs can be obtained as long as a reliable thermodynamic data are available for the binders being investigated. Steps for how to perform this method are illustrated in final section.

A large difference can be observed between the pore structure of hcp measured by water vapour sorption and N_2 sorption. This is mainly

derived from the effect of drying on the C-S-H structure and differences in diffusion kinetics. A severe drying treatment will induce a large contraction of C-S-H so that the interlayer channels are inaccessible for N_2. The underlying mechanism of the drying effect is illustrated by the colloidal globule model of C-S-H, and the effect of SCMs on the difference between water vapour and N_2 sorption has been comprehensively discussed.

CRediT authorship contribution statement

Liming Huang: Conceptualization, Methodology, Investigation, Data analysis, Writing-Original Draft, Writing-Review & Editing. *Luping Tang*: Methodology, Writing-Review & Editing, Supervision, Project administration, Funding acquisition. *Lars Wadsö*: Investigation, Writing-Review & Editing. *Ingemar Löfgren*: Investigation, Writing-Review & Editing. *Nilla Olsson*: Investigation, Project administration. *Zhenghong Yang*: Review & Editing, Supervision, Project administration.

Declaration of competing interest

We declare that there are no known competing financial interests or personal relationships that could have appeared to influence the work reported in this paper.

Data availability

Data will be made available on request.

Acknowledgements

References

[1] M.J. Abdolhosseini Qomi, L. Brochard, T. Honorio, I. Maruyama, M. Vandamme, Advances in atomistic modeling and understanding of drying shrinkage in cementitious materials, Cem. Concr. Res. 148 (2021), 106536, https://doi.org/10.1016/j.cemconres.2021.106536.

[2] P. Mehta, P. Monteiro, Concrete: Microstructure, Properties, and Materials, McGraw-Hill Education, 2014.

[3] H.M. Jennings, J.J. Thomas, J.S. Gevrenov, G. Constantinides, F.-J. Ulm, A multi-technique investigation of the nanoporosity of cement paste, Cem. Concr. Res. 37 (2007) 329–336, https://doi.org/10.1016/j.cemconres.2006.03.021.

[4] L. Huang, Water and alkali salts in the hydrating and hardened green cement-based materials: hydration process, moisture content and transport, Licentiate Thesis, Department of Civil Engineering, Chalmers University of Technology, 2022, https://research.chalmers.se/publication/528441/file/528441_Fulltext.pdf.

[5] P.J.M. Monteiro, G. Geng, D. Marchon, J. Li, P. Alapati, K.E. Kurtis, M.J.A. Qomi, Advances in characterizing and understanding the microstructure of cementitious materials, Cem. Concr. Res. 124 (2019), 105806, https://doi.org/10.1016/j.cemconres.2019.105806.

[6] M.D.A. Thomas, P.B. Bamforth, Modelling chloride diffusion in concrete effect of fly ash and slag, Cem. Concr. Res. 9 (1999).

[7] N. Olsson, F. Abdul Wahid, L.-O. Nilsson, C. Thiel, H.S. Wong, V. Baroghel-Bouny, Wick action in mature mortars with binary cements containing slag or silica fume – the relation between chloride and moisture transport properties under non-saturated conditions, Cem. Concr. Res. 111 (2018) 94–103, https://doi.org/10.1016/j.cemconres.2018.06.006.

[8] A. Korpa, R. Trettin, The influence of different drying methods on cement paste microstructures as reflected by gas adsorption: comparison between freeze-drying (F-drying), D-drying, P-drying and oven-drying methods, Cem. Concr. Res. 36 (2006) 634–649, https://doi.org/10.1016/j.cemconres.2005.11.021.

[9] H.M. Jennings, A. Kumar, G. Sant, Quantitative discrimination of the nano-pore-structure of cement paste during drying: new insights from water sorption isotherms, Cem. Concr. Res. 76 (2015) 27–36, https://doi.org/10.1016/j.cemconres.2015.05.006.

[10] M. Babaee, A. Castel, Water vapor sorption isotherms, pore structure, and moisture transport characteristics of alkali-activated and Portland cement-based binders, Cem. Concr. Res. 113 (2018) 99–120, https://doi.org/10.1016/j.cemconres.2018.07.006.

[11] N. De Belie, J. Kratky, S. Van Vlierberghe, Influence of pozzolans and slag on the microstructure of partially carbonated cement paste by means of water vapour and nitrogen sorption experiments and BET calculations, Cem. Concr. Res. 40 (2010) 1723–1733, https://doi.org/10.1016/j.cemconres.2010.08.014.

[12] D.N. Winslow, S. Diamond, Specific surface of hardened Portland cement paste as determined by small-angle X-ray scattering, J. Am. Ceram. Soc. 57 (1974) 193–197, https://doi.org/10.1111/j.1151-2916.1974.tb10856.x.

[13] J.J. Völkl, R.E. Beddoe, M.J. Setzer, The specific surface of hardened cement paste by small-angle X-ray scattering effect of moisture content and chlorides, Cem. Concr. Res. 17 (1987) 81–88, https://doi.org/10.1016/0008-8846(87)90062-7.

[14] A.J. Allen, J.J. Thomas, H.M. Jennings, Composition and density of nanoscale calcium–silicate–hydrate in cement, Nat. Mater. 6 (2007) 311–316.

[15] I. Maruyama, T. Ohkubo, T. Haji, R. Kurihara, Dynamic microstructural evolution of hardened cement paste during first drying monitored by 1H NMR relaxometry, Cem. Concr. Res. 122 (2019) 107–117, https://doi.org/10.1016/j.cemconres.2019.04.017.

[16] C. Zhou, F. Ren, Z. Wang, W. Chen, W. Wang, Why permeability to water is anomalously lower than that to many other fluids for cement-based material? Cem. Concr. Res. 100 (2017) 373–384, https://doi.org/10.1016/j.cemconres.2017.08.002.

[17] A.C.A. Muller, Characterization of porosity & CSH in cement pastes by 1H NMR, in: École polytechnique fédérale de Lausanne (EPFL), 2014. https://infoscience.epfl.ch/record/202011.

[18] C. Galle, Effect of drying on cement-based materials pore structure as identified by mercury intrusion porosimetry a comparative study between oven-, vacuum-, and freeze-drying, Cem. Concr. Res. 11 (2001).

[19] L.J. Parrott, W. Hansen, R.L. Berger, Effect of first drying upon the pore structure of hydrated alite paste, Cem. Concr. Res. 10 (1980) 647–655, https://doi.org/10.1016/0008-8846(80)90028-9.

[20] C. Zhou, X. Zhang, Z. Wang, Z. Yang, Water sensitivity of cement-based materials, J. Am. Ceram. Soc. 104 (2021) 4279–4296.

[21] D. Snoeck, L.F. Velasco, A. Mignon, S. Van Vlierberghe, P. Dubruel, P. Lodewyckx, N. De Belie, The effects of superabsorbent polymers on the microstructure of cementitious materials studied by means of sorption experiments, Cem. Concr. Res. 77 (2015) 26–35, https://doi.org/10.1016/j.cemconres.2015.06.013.

[22] Z. Zhang, G.W. Scherer, Evaluation of drying methods by nitrogen adsorption, Cem. Concr. Res. 120 (2019) 13–26, https://doi.org/10.1016/j.cemconres.2019.02.016.

[23] L.A. Tomes, C.M. Hunt, R.L. Blaine, Some factors affecting the surface area of hydrated Portland cement as determined by water-vapor and nitrogen adsorption, J. Res. Natl. Bur. Stan. 59 (1957) 357, https://doi.org/10.6028/jres.059.039.

[24] R.S. Mikhail, in: Adsorption of Organic Vapors in Relation to the, Special Report-Highway Research Board, 1966, p. 123.

[25] R.Sh. Mikhail, S.A. Abo-El-Enein, Studies on water and nitrogen adsorption on hardened cement pastes I development of surface in low porosity pastes, Cem. Concr. Res. 2 (1972) 401–414, https://doi.org/10.1016/0008-8846(72)90056-7.

[26] I. Odler, J. Hagymassy, M. Yudenfreund, K.M. Hanna, Pore structure analysis by water vapor adsorption IV. Analysis of hydrated Portland cement pastes of low porosity, J. Colloid Interface Sci. 38 (1972) 12.

[27] I. Odler, The BET-specific surface area of hydrated Portland cement and related materials, Cem. Concr. Res. 33 (2003) 2049–2056, https://doi.org/10.1016/S0008-8846(03)00225-4.

[28] H.M. Jennings, J.J. Thomas, A discussion of the paper "The BET-specific surface area of hydrated Portland cement and related materials" by Ivan odler, Cem. Concr. Res. 34 (2004) 1959–1960, https://doi.org/10.1016/j.cemconres.2004.03.001.

[29] V.Z. Zadeh, C.P. Bobko, Nanoscale mechanical properties of concrete containing blast furnace slag and fly ash before and after thermal damage, Cem. Concr. Compos. 37 (2013) 215–221.

[30] M.J. DeJong, F.-J. Ulm, The nanogranular behavior of C-S-H at elevated temperatures (up to 700 °C), Cem. Concr. Res. 37 (2007) 1–12, https://doi.org/10.1016/j.cemconres.2006.09.006.

[31] M. Sebastiani, R. Moscatelli, F. Ridi, P. Baglioni, F. Carassiti, High-resolution high-speed nanoindentation mapping of cement pastes: unravelling the effect of microstructure on the mechanical properties of hydrated phases, Mater. Des. 9 (2016).

[32] K.L. Scrivener, T. Füllmann, E. Gallucci, G. Walenta, E. Bermejo, Quantitative study of Portland cement hydration by X-ray diffraction/Rietveld analysis and independent methods, Cem. Concr. Res. 34 (2004) 1541–1547.

[33] K.L. Scrivener, B. Lothenbach, N. De Belie, E. Gruyaert, J. Skibsted, R. Snellings, A. Vollpracht, TC 238-SCM: hydration and microstructure of concrete with SCMs, Mater. Struct. 48 (2015) 835–862.

[34] R.A. Olson, H.M. Jennings, Estimation of CSH content in a blended cement paste using water adsorption, Cem. Concr. Res. 31 (2001) 351–356.

[35] L. Huang, L. Tang, I. Löfgren, N. Olsson, Z. Yang, Real-time monitoring the electrical properties of pastes to map the hydration induced microstructure

change in cement-based materials, Cem. Concr. Compos. 132 (2022), 104639, https://doi.org/10.1016/j.cemconcomp.2022.104639.

[36] L. Huang, L. Tang, I. Löfgren, N. Olsson, Z. Yang, Y. Li, Moisture and Ion Transport Properties in Blended Pastes and Their Relation to the Refined Pore Structure, Submitted to Cement and Concrete Research, 2022.

[37] B. Lothenbach, D.A. Kulik, T. Matschei, M. Balonis, L. Baquerizo, B. Dilnesa, G. D. Miron, R.J. Myers, Cemdata18: a chemical thermodynamic database for hydrated Portland cements and alkali-activated materials, Cem. Concr. Res. 115 (2019) 472–506, https://doi.org/10.1016/j.cemconres.2018.04.018.

[38] T. Thoenen, W. Hummel, U. Berner, E. Curti, The PSI/Nagra Chemical Thermodynamic Database 12/07, 2014.

[39] J.I. Escalante-García, J.H. Sharp, Effect of temperature on the hydration of the main clinker phases in Portland cements: part i, neat cements, Cem. Concr. Res. 28 (1998) 1245–1257, https://doi.org/10.1016/S0008-8846(98)00115-X.

[40] V. Baroghel-Bouny, Water vapour sorption experiments on hardened cementitious materials. Part II: Essential tool for assessment of transport properties and for durability prediction, Cem. Concr. Res. 37 (2007) 438–454, https://doi.org/10.1016/j.cemconres.2006.11.017.

[41] V. Baroghel-Bouny, Water vapour sorption experiments on hardened cementitious materials part I: essential tool for analysis of hygral behaviour and its relation to pore structure, Cem. Concr. Res. 37 (2007) 414–437, https://doi.org/10.1016/j.cemconres.2006.11.019.

[42] O. Linderoth, P. Johansson, L. Wadsö, Development of pore structure, moisture sorption and transport properties in fly ash blended cement-based materials, Constr. Build. Mater. 261 (2020), 120007, https://doi.org/10.1016/j.conbuildmat.2020.120007.

[43] N. Olsson, L.-O. Nilsson, M. Åhs, V. Baroghel-Bouny, Moisture transport and sorption in cement based materials containing slag or silica fume, Cem. Concr. Res. 106 (2018) 23–32, https://doi.org/10.1016/j.cemconres.2018.01.018.

[44] Y. Xi, Z.P. Bažant, L. Molina, H.M. Jennings, Moisture diffusion in cementitious materials moisture capacity and diffusivity, Adv. Cem. Based Mater. 1 (1994) 258–266.

[45] I. Maruyama, J. Rymeš, M. Vandamme, B. Coasne, Cavitation of water in hardened cement paste under short-term desorption measurements, Mater. Struct. 51 (2018) 159, https://doi.org/10.1617/s11527-018-1285-x.

[46] M. Rastogi, A. Müller, M.B. Haha, K.L. Scrivener, The role of cavitation in drying cementitious materials, Cem. Concr. Res. 154 (2022), 106710, https://doi.org/10.1016/j.cemconres.2022.106710.

[47] S. Brunauer, P.H. Emmett, E. Teller, Adsorption of gases in multimolecular layers, J. Am. Chem. Soc. 60 (1938) 309–319, https://doi.org/10.1021/ja01269a023.

[48] J. Hagymassy Jr., S. Brunauer, R.S. Mikhail, Pore structure analysis by water vapor adsorption: I. T-curves for water vapor, J. Colloid Interface Sci. 29 (1969) 485–491.

[49] J. Hagymassy Jr., I. Odler, M. Yudenfreund, J. Skalny, S. Brunauer, Pore structure analysis by water vapor adsorption. III. Analysis of hydrated calcium silicates and Portland cements, J. Colloid Interface Sci. 38 (1972) 20–34.

[50] R. Tišlova, A. Kozłowska, R. Kozłowski, D. Hughes, Porosity and specific surface area of Roman cement pastes, Cem. Concr. Res. 39 (2009) 950–956, https://doi.org/10.1016/j.cemconres.2009.06.020.

[51] R.W. Mooney, A.G. Keenan, L.A. Wood, Adsorption of water vapor by montmorillonite. I. Heat of desorption and application of BET theory, J. Am. Chem. Soc. 74 (1952) 1367–1371, https://doi.org/10.1021/ja01126a001.

[52] R.W. Mooney, A.G. Keenan, L.A. Wood, Adsorption of water vapor by montmorillonite. II. Effect of exchangeable ions and lattice swelling as measured by X-ray diffraction, J. Am. Chem. Soc. 74 (1952) 1371–1374, https://doi.org/10.1021/ja01126a002.

[53] I. Odler, H.-P. Barthold, in: Investigations On The Water Vapor Permeability Of Cementitious Materials Ivan Odler And Hans-Peter Barthold, MRS Online Proceedings Library (OPL), 1988, p. 137.

[54] C. Roosz, S. Gaboreau, S. Grangeon, D. Prêt, V. Montouillout, N. Maubec, S. Ory, P. Blanc, P. Vieillard, P. Henocq, Distribution of water in synthetic calcium silicate hydrates, Langmuir 32 (2016) 6794–6805, https://doi.org/10.1021/acs.langmuir.6b00878.

[55] P. Bayliss, Further interlayer desorption studies of CSH(1), Cem. Concr. Res. 3 (1973) 185–188, https://doi.org/10.1016/0008-8846(73)90046-X.

[56] R.H. Smith, P. Bayliss, Interlayer desorption of CSH(1), Cem. Concr. Res. 2 (1972) 643–646, https://doi.org/10.1016/0008-8846(72)90001-4.

[57] L.J. Parrott, J.F. Young, Effect of prolonged drying upon the silicate structure of hydrated alite pastes, Cem. Concr. Res. 11 (1981) 11–17, https://doi.org/10.1016/0008-8846(81)90004-1.

[58] A. Bentur, R.L. Berger, F. Lawrence Jr., N. Milestone, S. Mindess, J.F. Young, Creep and drying shrinkage of calcium silicate pastes III. A hypothesis of irreversible strains, Cem. Concr. Res. 9 (1979) 83–95.

[59] R.F. Feldman, Helium flow characteristics of rewetted specimens of dried hydrated Portland cement paste, Cem. Concr. Res. 3 (1973) 777–790.

[60] H.M. Jennings, A model for the microstructure of calcium silicate hydrate in cement paste, Cem. Concr. Res. 30 (2000) 101–116, https://doi.org/10.1016/S0008-8846(99)00209-4.

[61] E.P. Barrett, L.G. Joyner, P.P. Halenda, The determination of pore volume and area distributions in porous substances. I. Computations from nitrogen isotherms, J. Am. Chem. Soc. 73 (1951) 373–380.

[62] E.A. Guggenheim, The theoretical basis of Raoult's law, Trans. Faraday Soc. 33 (1937) 151, https://doi.org/10.1039/tf9373300151.

[63] H. Chen, M. Wyrzykowski, K. Scrivener, P. Lura, Prediction of self-desiccation in low water-to-cement ratio pastes based on pore structure evolution, Cem. Concr. Res. 49 (2013) 38–47, https://doi.org/10.1016/j.cemconres.2013.03.013.

[64] S.-Y. Hong, F.P. Glasser, Alkali binding in cement pastes: part I. The CSH phase, Cem. Concr. Res. 29 (1999) 1893–1903.

[65] R. Badmann, N. Stockhausen, M.J. Setzer, The statistical thickness and the chemical potential of adsorbed water films, J. Colloid Interface Sci. 82 (1981) 534–542, https://doi.org/10.1016/0021-9797(81)90395-7.

[66] H.M. Jennings, Refinements to colloid model of C-S-H in cement: CM-II, Cem. Concr. Res. 38 (2008) 275–289, https://doi.org/10.1016/j.cemconres.2007.10.006.

[67] A.C.A. Muller, K.L. Scrivener, A.M. Gajewicz, P.J. McDonald, Densification of C-S–H measured by 1 H NMR relaxometry, J. Phys. Chem. C 117 (2013) 403–412, https://doi.org/10.1021/jp3102964.

[68] G.W. Scherer, D.M. Smith, Cavitation during drying of a gel, J. Non-Cryst. Solids 189 (1995) 197–211, https://doi.org/10.1016/0022-3093(95)00222-7.

[69] M. Thommes, B. Smarsly, M. Groenewolt, P.I. Ravikovitch, A.V. Neimark, Adsorption hysteresis of nitrogen and argon in pore networks and characterization of novel micro- and mesoporous silicas, Langmuir 22 (2006) 756–764, https://doi.org/10.1021/la051686h.

[70] J.I. Escalante-Garcia, Nonevaporable water from neat OPC and replacement materials in composite cements hydrated at different temperatures, Cem. Concr. Res. 33 (2003) 1883–1888, https://doi.org/10.1016/S0008-8846(03)00208-4.

[71] L. Lam, Y.L. Wong, C.S. Poon, Degree of hydration and gel/space ratio of high-volume fly ash/cement systems, Cem. Concr. Res. 30 (2000) 747–756, https://doi.org/10.1016/S0008-8846(00)00213-1.

[72] C. Zhou, F. Ren, Q. Zeng, L. Xiao, W. Wang, Pore-size resolved water vapor adsorption kinetics of white cement mortars as viewed from proton NMR relaxation, Cem. Concr. Res. 105 (2018) 31–43, https://doi.org/10.1016/j.cemconres.2017.12.002.

[73] P.A. Bonnaud, Q. Ji, B. Coasne, R.J.-M. Pellenq, K.J. Van Vliet, Thermodynamics of water confined in porous calcium-silicate-hydrates, Langmuir 28 (2012) 11422–11432, https://doi.org/10.1021/la301738p.

[74] R.J.-M. Pellenq, A. Kushima, R. Shahsavari, K.J. Van Vliet, M.J. Buehler, S. Yip, F.-J. Ulm, A realistic molecular model of cement hydrates, Proc. Natl. Acad. Sci. U. S. A. 106 (2009) 16102–16107, https://doi.org/10.1073/pnas.0902180106.

[75] G. Kovačević, B. Persson, L. Nicoleau, A. Nonat, V. Veryazov, Atomistic modeling of crystal structure of ca 1.67 SiH x, Cem. Concr. Res. 67 (2015) 197–203, https://doi.org/10.1016/j.cemconres.2014.09.003.

[76] I.G. Richardson, Tobermorite/jennite- and tobermorite/calcium hydroxide-based models for the structure of C-S-H: applicability to hardened pastes of tricalcium silicate, β-dicalcium silicate, Portland cement, and blends of Portland cement with blast-furnace slag, metakaolin, or silica fume, Cem. Concr. Res. 34 (2004) 1733–1777, https://doi.org/10.1016/j.cemconres.2004.05.034.

[77] O.M. Jensen, P.F. Hansen, Water-entrained cement-based materials I. Principles and theoretical background, Cem. Concr. Res. 34 (2001) 647–654.

[78] J. Skibsted, R. Snellings, Reactivity of supplementary cementitious materials (SCMs) in cement blends, Cem. Concr. Res. 124 (2019), 105799, https://doi.org/10.1016/j.cemconres.2019.105799.

[79] K. De Weerdt, M.B. Haha, G. Le Saout, K.O. Kjellsen, H. Justnes, B. Lothenbach, Hydration mechanisms of ternary Portland cements containing limestone powder and fly ash, Cem. Concr. Res. 41 (2011) 279–291, https://doi.org/10.1016/j.cemconres.2010.11.014.

[80] A. Schöler, B. Lothenbach, F. Winnefeld, M. Zajac, Hydration of quaternary Portland cement blends containing blast-furnace slag, siliceous fly ash and limestone powder, Cem. Concr. Compos. 55 (2015) 374–382, https://doi.org/10.1016/j.cemconcomp.2014.10.001.

[81] B. Lothenbach, M. Zajac, Application of thermodynamic modelling to hydrated cements, Cem. Concr. Res. 123 (2019), 105779, https://doi.org/10.1016/j.cemconres.2019.105779.

[82] B.Z. Dilnesa, E. Wieland, B. Lothenbach, R. Dähn, K.L. Scrivener, Fe-containing phases in hydrated cements, Cem. Concr. Res. 58 (2014) 45–55, https://doi.org/10.1016/j.cemconres.2013.12.012.

[83] F. Deschner, B. Lothenbach, F. Winnefeld, J. Neubauer, Effect of temperature on the hydration of Portland cement blended with siliceous fly ash, Cem. Concr. Res. 52 (2013) 169–181, https://doi.org/10.1016/j.cemconres.2013.07.006.

[84] S. Adu-Amankwah, M. Zajac, C. Stabler, B. Lothenbach, L. Black, Influence of limestone on the hydration of ternary slag cements, Cem. Concr. Res. 100 (2017) 96–109, https://doi.org/10.1016/j.cemconres.2017.05.013.

[85] E. L'Hôpital, B. Lothenbach, G. Le Saout, D. Kulik, K. Scrivener, Incorporation of aluminium in calcium-silicate-hydrates, Cem. Concr. Res. 75 (2015) 91–103, https://doi.org/10.1016/j.cemconres.2015.04.007.

[86] M.B. Haha, K. De Weerdt, B. Lothenbach, Quantification of the degree of reaction of fly ash, Cem. Concr. Res. 40 (2010) 1620–1629.

[87] V. Kocaba, E. Gallucci, K.L. Scrivener, Methods for determination of degree of reaction of slag in blended cement pastes, Cem. Concr. Res. 42 (2012) 511–525, https://doi.org/10.1016/j.cemconres.2011.11.010.

[88] Z.C. Grasley, D.A. Lange, Thermal dilation and internal relative humidity of hardened cement paste, Mater. Struct. 40 (2007) 311–317, https://doi.org/10.1617/s11527-006-9108-x.

[89] R.B. Kogbara, S.R. Iyengar, Z.C. Grasley, E.A. Masad, D.G. Zollinger, A review of concrete properties at cryogenic temperatures: towards direct LNG containment, Constr. Build. Mater. 47 (2013) 760–770, https://doi.org/10.1016/j.conbuildmat.2013.04.025.

[90] E.S. Boek, P.V. Coveney, N.T. Skipper, Monte Carlo molecular modeling studies of hydrated li-, na-, and K-smectites: understanding the role of potassium as a clay swelling inhibitor, J. Am. Chem. Soc. 117 (1995) 12608–12617, https://doi.org/10.1021/ja00155a025.

[91] E. Xie, C. Zhou, Q. Song, Q. Zeng, Z. Wang, The effect of chemical aging on water permeability of white cement mortars in the context of sol–gel science, Cem. Concr. Compos. 114 (2020), 103812, https://doi.org/10.1016/j.cemconcomp.2020.103812.

[92] W.-S. Chiang, E. Fratini, P. Baglioni, D. Liu, S.-H. Chen, Microstructure determination of calcium-silicate-hydrate globules by small-angle neutron scattering, J. Phys. Chem. C 116 (2012) 5055–5061, https://doi.org/10.1021/jp300745g.

[93] A.S. Ziarani, R. Aguilera, Knudsen's permeability correction for tight porous media, Transp. Porous Media 91 (2012) 239–260, https://doi.org/10.1007/s11242-011-9842-6.

[94] D.W. Breck, D.W. Breck, Zeolite Molecular Sieves: Structure, Chemistry, and Use, John Wiley & Sons, 1973.

[95] J. Du, A. Zhou, S.-L. Shen, X. Lin, Y. Bu, J. Kodikara, Revealing crucial effects of temperature and salinization on swelling behavior of montmorillonite, Chem. Eng. J. 429 (2022), 132263, https://doi.org/10.1016/j.cej.2021.132263.

[96] R. Kurihara, I. Maruyama, Revisiting tennis-Jennings method to quantify low-density/high-density calcium silicate hydrates in Portland cement pastes, Cem. Concr. Res. 156 (2022), 106786, https://doi.org/10.1016/j.cemconres.2022.106786.

[97] M. Yi, Y. Cheng, Z. Wang, C. Wang, B. Hu, X. He, Effect of particle size and adsorption equilibrium time on pore structure characterization in low pressure

[98] R. Taylor, I.G. Richardson, R.M.D. Brydson, Composition and microstructure of 20-year-old ordinary Portland cement–ground granulated blast-furnace slag blends containing 0 to 100% slag, Cem. Concr. Res. 40 (2010) 971–983, https://doi.org/10.1016/j.cemconres.2010.02.012.

[99] N. Iyi, K. Fujii, K. Okamoto, T. Sasaki, Factors influencing the hydration of layered double hydroxides (LDHs) and the appearance of an intermediate second staging phase, Appl. Clay Sci. 35 (2007) 218–227, https://doi.org/10.1016/j.clay.2006.08.011.

[100] E. Bernard, W.J. Zucha, B. Lothenbach, U. Mäder, Stability of hydrotalcite (Mg-Al layered double hydroxide) in presence of different anions, Cem. Concr. Res. 152 (2022), 106674, https://doi.org/10.1016/j.cemconres.2021.106674.

[101] S. Diamond, J.L. White, W.L. Dolch, Effects of isomorphous substitution in hydrothermally-synthesized tobermorite, Am. Mineral. 51 (1966) 388–401.

[102] S.A. Greenberg, Calcium silicate hydrate (I), J. Phys. Chem. 58 (1954) 362–367.

[103] G. Geng, R.J. Myers, J. Li, R. Maboudian, C. Carraro, D.A. Shapiro, P.J.M. Monteiro, Aluminum-induced dreierketten chain cross-links increase the mechanical properties of nanocrystalline calcium aluminosilicate hydrate, Sci. Rep. 7 (2017) 44032, https://doi.org/10.1038/srep44032.

N2 adsorption of coal: an experimental study, Adv. Powder Technol. 31 (2020) 4275–4281, https://doi.org/10.1016/j.apt.2020.09.004.